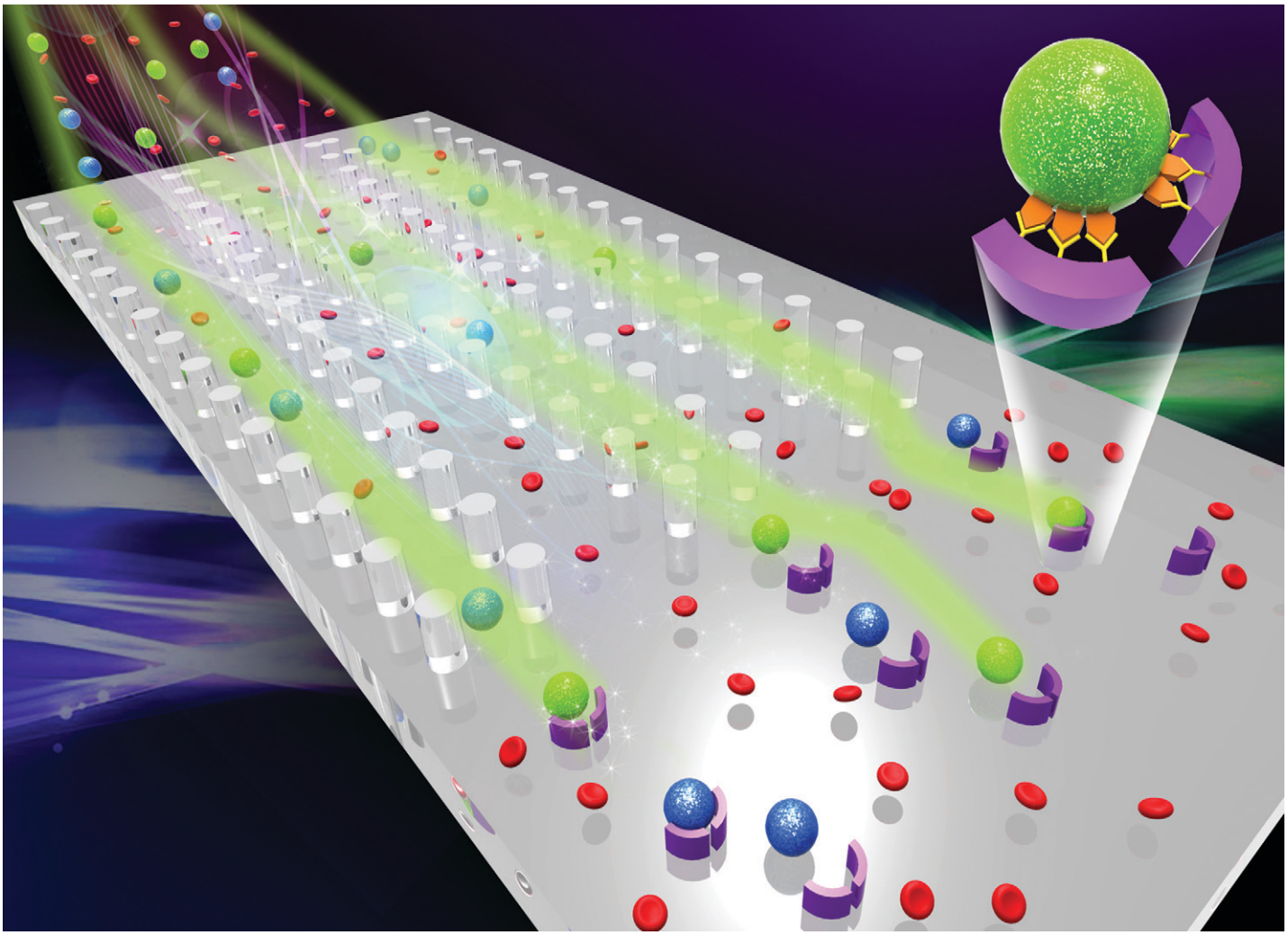

Showcasing research from Professor Raymond H. W. Lam's laboratory, City University of Hong Kong Shenzhen Research Institute, Shenzhen, China.

Antibody-coated microstructures for selective isolation of immune cells in blood

A microstructured device has been developed for achieving high-yield selective isolation of target immune cells from blood, supporting downstream genetic and biochemical cell analyses, and contributing to the medical diagnosis of a broad range of immune diseases. Taking cell-structure interactions into account, arrays of micropillars and micro-sieves are placed with optimized arrangements. Surface modification offers selective cell capture in the micro-sieves based on antigen-antibody bindings. This device can achieve a selective cell isolation yield of >80%, cell purity of ~100% and cell viability of >93%.

As featured in:

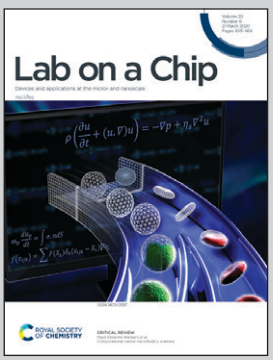

See Raymond H. W. Lam *et al.*, *Lab Chip*, 2020, **20**, 1072.

ROYAL SOCIETY OF CHEMISTRY

rsc.li/loc

Registered charity number: 207890

Lab on a Chip

ROYAL SOCIETY OF CHEMISTRY

PAPER

View Article Online
View Journal | View Issue

Check for updates

Cite this: *Lab Chip*, 2020, **20**, 1072

Antibody-coated microstructures for selective isolation of immune cells in blood†

Jiyu Li,‡[a] Ya Liu,‡[a] Jifeng Ren,[a] Benjamin Zikai Tay,[b] Tao Luo,[a] Lei Fan,[a] Dong Sun,[ac] Guannan Luo,[d] Denvid Lau,[e] Marcos[b] and Raymond H. W. Lam *[acfg]

Received 23rd January 2020,
Accepted 9th February 2020

DOI: 10.1039/d0lc00078g

rsc.li/loc

Cell isolation from blood is an important process for diagnosing immune diseases. There are still demands for a user-friendly approach to achieve high cell extraction efficiency and purity of a target immune cell subtype for more promising diagnosis and monitoring. For selective immune cell isolation, we developed a microstructured device, which consists of antibody-coated micropillars and micro-sieve arrays, for isolating a target immune cell subtype from bovine blood samples. The focusing micropillars can guide immune cells flowing to the subsequent micro-sieves based on deterministic lateral shifts of the cells. The arrangement of these microstructures is characterized and configured for the maximal cell capture rate. Surface modification with a selected antibody offers selective cell capture in the micro-sieves based on the antigen–antibody reaction. We prepare a cell mixture of human CD14-expressing leukemia cells (THP-1) and epithelial cells (MDA-MB-231) in diluted blood to characterize the cell isolation operation, with a selective cell isolation yield of >80%, cell purity of ~100% and cell viability of >93%. Together, this microstructured device strategy can achieve high-yield selective isolation of immune cells from blood samples and support downstream genetic and biochemical cell analyses, contributing to the medical diagnosis of a broad range of immune diseases.

Introduction

Immune system diseases, such as human immunodeficiency virus (HIV) infection, tuberculosis, malaria, and sepsis, can be fatal.[1] Many of these diseases are subject to particular abnormal immune cell subtypes,[2] yet the presence of heterogeneous cell subtypes in blood causes the accurate identification and characterization of these abnormal cells very challenging.[3] Cytokines, as the key cell signaling molecules, secreted by each immune cell subtype can reflect the immune status, especially for immune disease patients. However, the cytokine secretion dynamics of each subtype in blood samples could not be quantified because the direct cytokine levels in a blood sample are contributed by all the cell subtypes, rather than a specific subtype.[4] Hence, selective isolation of an immune cell subtype is of vital importance to the investigation of patients' immune status.

Generally, selective cell isolation of heterogeneous cell mixtures is an essential operation in clinical diagnostics, monitoring and therapeutics, and other cell processing methods.[5] Although there are some physical isolation techniques, such as centrifugal sedimentation and cell electrophoresis,[6] the cell-type purity obtained by these methods are comparatively low.[7] Many other techniques are based on immune-affinity.[8] Material surfaces have been coated with an antibody such that cells with the matching surface protein could be captured *via* antibody–protein binding.[9] A well-known commercially available technique is using antibody-coated magnetic microbeads, with which a magnetic field can be applied to extract bound target cells. Though very effective,[10] removal of the magnetic microbeads is challenging, limiting the compatibility of the follow-up cell culture and analysis approaches. Perozziello *et al.* applied a membrane coated with the anti-HLA (human leukocyte antigen) class I antibody for capturing human nucleated blood cells including immune cells.[11] An anti-EpCAM (epithelial cell adhesion molecule) antibody coated nano-thick film was demonstrated to separate

[a] *Department of Biomedical Engineering, City University of Hong Kong, Hong Kong. E-mail: rhwlam@cityu.edu.hk; Fax: +852 3442 0172; Tel: +852 3442 8577*
[b] *School of Mechanical and Aerospace Engineering, Nanyang Technological University, Singapore*
[c] *Centre for Robotics and Automation, City University of Hong Kong, Hong Kong*
[d] *Department of Economics and Finance, City University of Hong Kong, Hong Kong*
[e] *Department of Architecture and Civil Engineering, City University of Hong Kong, Hong Kong*
[f] *Centre for Biosystems, Neuroscience, and Nanotechnology, City University of Hong Kong, Hong Kong*
[g] *City University of Hong Kong Shenzhen Research Institute, Shenzhen, China*

† Electronic supplementary information (ESI) available. See DOI: 10.1039/d0lc00078g

‡ These authors equally contributed to this work.

circulating gastric cancer cells from colorectal and peripheral blood samples.[12] Fan *et al.* presented a combination of antibodies and aptamers as a multivalent adhesive domain for target cancer cell types.[13]

Microstructures integrated with immune-affinity surfaces have been widely recognized as powerful functional materials for specific cell isolation,[14] largely because such a strategy can further offer micro-scale cell trappers with larger surface areas for higher cell capture rates.[15] For example, Rodriguez *et al.* applied filtration membranes to isolate CD4+ T cells directly from unlabeled blood from patients infected with HIV.[16] A microfabricated micro-porous membrane with an antibody-coating could rapidly filter target immune cells adhering on antibody-coated micro-beads[17] based on the avidin–biotin coating process.[18] Anti-EpCAM-coated micropillar structures were applied in capturing circulating tumor cells from cancer patients.[19] An antibody-coated micropillar array has also demonstrated the effective isolation of lung cancer cells.[20] Generally, a higher density and larger total surface area of the microstructures can reach a higher cell capture rate, yet it would also induce the difficult extraction of attached cells for any subsequent analyses.

In fact, hydrodynamic effects can vary the trajectory of cells flowing around microstructures,[21] including immune cells in blood.[22] It has been reported that the dimensions and placement of the microstructures can be finely tuned to enhance the cell–structure contact frequency.[23] Warkiani *et al.* presented size-based cell isolation using a label-free spiral microchannel, in which the lateral cell positions were shifted by hydrodynamic force in curvilinear flow.[24] A wavy-herringbone micro-structured surface coated with antibodies was also reported for cancer cell isolation from blood samples[25] by inducing lateral flow on the micro-structures for enhancing cell–structure contact. Nevertheless, the cell attachment sites are highly random and hence locating cells for any cell identification and analysis directly in the device can be challenging. Recently, we have also reported the optimized placement of micro-sieves for sequential cell capture[26] based on the alternative lateral shifts of cells from a defined upstream lateral location. This strategy achieved a reasonably high capture rate of >90% of single-cells at defined positions in the device, and it allowed cell extraction out from the device for any further analyses. The micro-sieve surfaces can be further coated with an antibody targeting a cell surface protein for selective cell isolation, for selective binding and extraction of the target immune cell subtype. While they captured floating cells very effectively, the operation was not straightforward. Technically, this method required additional flows of the culture medium/buffer solution to focus cells along the micro-sieve positions during operation, which heavily diluted the cell density and limited the throughput. In other words, this strategy should be further improved for better applicability to practical immune cell isolation.

In this work, we present the development of an antibody-coated micro-sieve array integrated with focusing pillars for selective immune cell isolation from blood. Upstream micro-pillars are added for shifting the immune cells to the functioning range of lateral locations for the subsequent cell capture. This strategy of integrating micro-pillars offers a simple cell focusing and isolation scheme, such that the resultant device includes only one inlet and one outlet. The biosamples can be directly injected along the microstructures without additional flows of buffer solutions, resulting in a higher applicability to immune cell isolation from blood. Such a simplified operation further allows duplication of the microstructures in parallel for a significantly higher throughput, meeting the requirements for clinical implementation.

Materials and methods

Fabrication

The device fabrication was based on photolithography and replica molding of polydimethylsiloxane (PDMS; Sylgard-184, Dow Corning, Midland, MI, USA). The design layout was designed with computer graphics software (AutoCAD, Autodesk, USA) and transferred as chrome masks (New Way Photomask, Shenzhen, China). The mold was fabricated by patterning SU-8 photoresist (SU-8 2015, Microchem) with a thickness of 30 μm on a silicon wafer. The mold was salinized by depositing a molecular layer of trichloro-(1*H*,1*H*,2*H*,2*H*-perfluorooctyl) silane (Sigma-Aldrich, St. Louis, MO) to facilitate the release of PDMS from the mold master in the later steps. After the mold fabrication, the PDMS monomer was mixed with the curing agent in a weight ratio of 10 : 1; and the mixture was degassed in a vacuum environment for 3–5 min. The degassed PDMS mixture was poured onto the control layer mold with a thickness of 3 mm. After baking in an oven at 80 °C for 20 min, the PDMS substrate was chopped and peeled-off from its mold, followed by punching holes (diameter: 0.5 mm; WHAWB100073, Sigma-Aldrich) at the device inlet and outlet. The PDMS substrate was then bonded onto a glass slide using oxygen plasma treatment (energy: 5 kJ; Harrick plasma cleaner PDC-002). We further baked the device at 100 °C for >20 h and applied ultraviolet irradiation for 2 h for sterilization before any device operation.

Antibody coating and device preparation

All the surfaces of the microstructures in the device were functionalized with antibodies against CD14 based on the avidin–biotin reaction.[18,27] We injected (3-mercaptopropyl)-trimethoxysilane (Gelest, Morrisville, PA)[28] in ethanol with a volume ratio of 1 : 25 (v/v) into the device for 30 min at 37 °C, followed by flushing the flow channels with pure ethanol. We then injected 0.28% (w/v) *N*-(γ-maleimidobutyryloxy)-succinimide ester (GMBS)[29,30] in ethanol into the device for 15 min for the molecular coating. After flushing the flow channels with 1× phosphate buffered saline (PBS; Welgene, Korea), 10 μg ml^{-1} avidin (434401, Life Technologies, Grand Island, NY)[31] was further injected into the device and stayed for 30 min. The flow region was then rinsed with 1× PBS

again, and CD14 monoclonal antibodies (Life Technologies, Grand Island, NY)[32] were finally injected into the device for 10 min for the antibody coating.

Microscope and device setup

We utilized an inverted fluorescence microscope (TE300, Nikon, Tokyo, Japan) installed with an sCMOS camera (Zyla 4.2, Andor, Belfast, UK), a stage heater with temperature control, and a chamber filled with 5% CO_2 in air. Before the cell isolation operation, we placed the device on the microscope stage under stable temperature (37 °C), humidity (saturated) and gas (5% CO_2) conditions for at least 30 min. Syringe tubing (Tygon™ tubing, US Plastics, Lima, OH) was inserted into the device inlet and outlet. In particular, the syringe tubing for the sample inlet was pre-filled with the cell sample, and its upstream end was connected to pressure regulators to supply adjustable inlet pressures for driving the liquid flow during the cell isolation operation.

Cell culture

Human monocytic leukemia cells (THP-1; TIB-202, ATCC) with an average cell diameter of ~15 μm were maintained in RPMI-1640 medium containing 10% FBS (Thermo Fisher Scientific, Inc., Pittsburgh, PA, USA), 1% penicillin (Life Technologies, Singapore), and 0.05 mM 2-mercaptoethanol (Sigma-Aldrich, St. Louis, MO). On the other hand, MDA-MB-231 cells (HTB-26, ATCC) with an average diameter of ~17 μm were cultured in DMEM–F12 (Sigma-Aldrich, St. Louis, MO) with 10% FBS and 1% penicillin added. All cells were cultured in an incubator (HERAcell 150, Heraeus, Germany) at 37 °C in a 5% CO_2 environment.

Blood sample preparation

Bovine whole blood samples (HongQuan Bio Co., Ltd, China) were first filtered using a nylon syringe filter with a pore size of 5 μm (Whatman 6871-2550 GD/X, GE Healthcare Life Sciences, USA) to eliminate the white blood cells and any bigger cells. In addition, we applied flow cytometry to verify that the filtered samples contained no cells with a diameter of >7 μm. The filtered samples were then diluted in PBS with 1% bovine serum albumin (BSA; Sigma-Aldrich, MO). The hematocrit levels were measured as the volume ratio of the packed red blood cells to the whole blood in a capillary tube after centrifugation.

Cell viability tests

We performed cell viability tests for the isolated cells directly inside the device. We injected the reagents from a LIVE/DEAD cell viability kit (cat # L-3224, Life Technologies)[33–36] into the sample inlet which were maintained for 30 min to stain the isolated cells with fluorescent dyes (GFP for live cells and Cy3 for dead cells). Fluorescence microscopic images were then captured under a microscope.

On the other hand, we also performed cell viability tests on the extracted target cells. After the target cells were selectively isolated and released from the device, we transferred the extracted cells to a 200 μl syringe tube. We applied the reagents from the LIVE/DEAD cell viability kit to the extracted cells with incubation of 30 min, followed by counting the live (GFP) and dead (Cy3) cells using flow cytometry.

Live subject statement

All the experiments were performed in compliance with the Animals (Control of Experiments) Ordinance (Cap. 340) licensed by the Department of Health of the Hong Kong Government [reference no. (18-6) in DH/SHS/8/2/5 Pt.3]. All the experimental procedures were approved by the Committee on the Use and Care of Animals at City University of Hong Kong.

Flow simulation

We performed numerical simulation using commercial software (COMSOL Multiphysics, COMSOL, Burlington, MA) to quantify the streamlines in the immune cell isolation chip.[37] Considering that the liquid flow rate was ~0.75 μl min^{-1} and the velocity was ~625 μm s^{-1} in the device with a characteristic length of ~10 μm, corresponding to the Reynolds number, Re ~0.00625, we applied a laminar flow model for solving the Navier–Stokes equations.

Statistics

All error bars in the plots are standard errors. All experiments were conducted with at least 8 independent experiments. An asterisk in a plot represents a statistically significant difference between two data groups (p-value < 0.05). P-Values are determined by comparing two groups of data using two-tailed, unpaired Student's t-test.

Results and discussion

Device design and operation

To achieve isolation of target immune cells from the biosamples, we have developed and fabricated a microfluidic device (Fig. 1a) containing two regions of microstructure arrays with surface modification for capturing target immune cells with a defined surface protein expression. The first region is an array of micropillars for cell focusing while the second stage is an array of micro-sieves for cell capture as shown in Fig. 1b. The device has an inlet and an outlet connecting to these two micro-structured regions (total volume: ~1 μl).

In this work, the microstructures were configured for isolating THP-1 cells with an average diameter of 14.36 ± SD 1.48 μm (quantified by flow cytometry as shown in Fig. S1†). The focusing region is an array of cylindrical micropillars with a diameter of 50 μm. Between consecutive micropillars along the flow direction, the center–center distance along the flow is 70 μm and the lateral offset distance is 1 μm. We have configured two columns of the 35 micropillars with the same

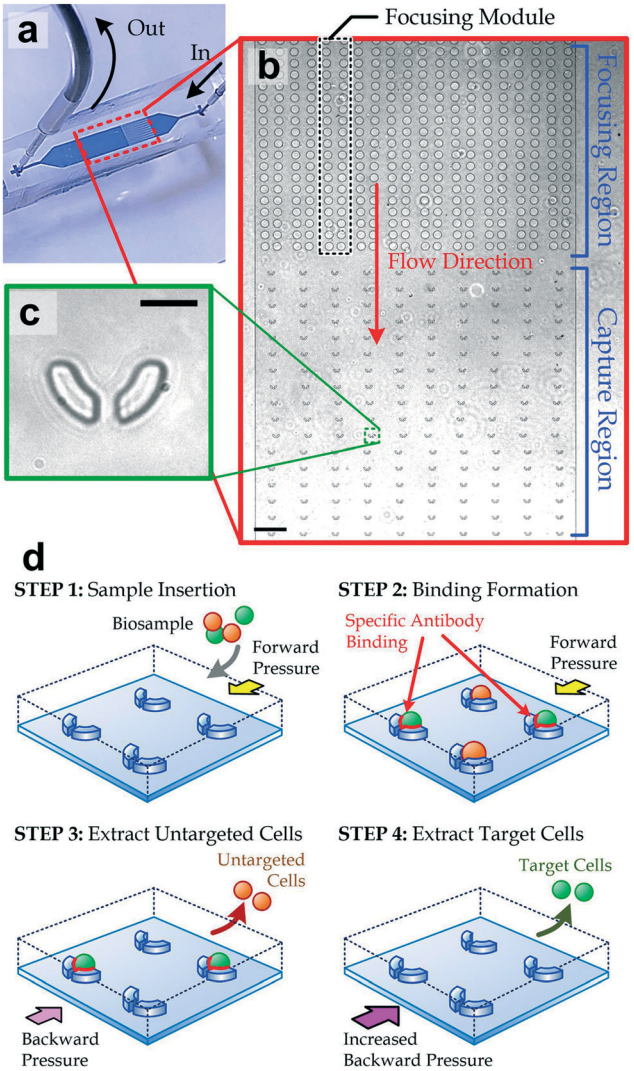

Fig. 1 (a) Photograph of the fabricated immune cell isolation device with its inlet and outlet connected with tubing. The flow channel is filled with a blue dye for better visualization. (b) Focusing region and capture region in the device. Only parts of the regions are shown here, as the focusing region has 35 rows of micropillars and the capture region only shows 20 rows of micro-sieves in total. The focusing region can be considered as 10 copies of the focusing modules. Scale bar: 200 μm. (c) One micro-sieve structure. Scale bar: 20 μm. (d) Procedures of specific cell isolation operation.

distance but opposite directions of the lateral offsets to be grouped into a focusing module (Fig. 1b). The first micropillars in both the pillar-columns (with a center–center separating distance of 130 μm) act as the entrance of the focusing module. For the following micropillars, their lateral center–center separating distance reduces gradually down to 72 μm for the last adjacent micropillar pair, generating an exit gap of one cell focusing module of 22 μm. When an immune cell (typically with a diameter of 10–18 μm) flows along the focusing region, the immune cell should be focused to the module exit. Considering that the immune cells have a range of diameters, it should be mentioned that the exit gap (22 μm) is larger than all the immune cells without causing any cell deformation or even cell congestion; and therefore the cells still have a range of possible lateral positions after passing the focusing modules. As the device contains ten focusing modules, the cells can be guided to specific lateral locations at one of the focusing module exits, which is critical for the following cell capture process. The capture region consists of multiple (twenty) rows of micro-sieves (ten micro-sieves in each row), with each having the microstructure as we have previously reported.[26] Each micro-sieve is a semicircular wall (inner diameter: 30 μm; outer diameter: 40 μm) with a gap (width: 6 μm) at the wall center, functioning as a cell trapper (Fig. 1c). The presence of a cell in a micro-sieve varies the flow profiles around the micro-sieve, forcing the next cell to flow around the micro-sieve with a lateral offset and be isolated in the downstream micro-sieve. We have optimized the arrangement of the micro-sieves for a higher cell capture rate, *i.e.* the number of cells captured in the micro-sieves relative to the total injected cells. Between two consecutive micro-sieves along each row in the current device, the center–center separating distance along the flow is 100 μm and the center–center lateral offsets are in the range of −30 μm to 30 μm (the detailed configuration is listed in ESI† Table S1), relative to the lateral center position of the upstream focusing module exit. It should be noted that a specific binding can be formed between the antibody-coated micro-sieve and the target cell expressing the specific surface protein.

The microfluidic device can implement the specific cell isolation following the procedures described in Fig. 1d. A biosample should first be loaded into the device with a steady driving pressure. Ideally, all the immune cells are focused and trapped in the micro-sieves (step 1); whereas other smaller cells, *e.g.* red blood cells and blood platelets, can then be removed by asubsequent flush of culture media. The captured target immune cells are incubated for 10 min with the antibody-coated micro-sieves for specific protein–antibody binding (step 2). Next, we inject fresh culture media from the outlet with a controlled pressure level such that the backward flow can remove all the unbound cells (step 3). Lastly, we can increase the backward flow pressure to extract the target immune cells for further cell analyses (step 4).

Microstructure arrangements

The working principle of the cell isolation operation is based on the effects of the microstructures on the cell trajectories. For the cell focusing, we considered a cell (diameter: 10 μm) flowing along the streamlines which would exhibit lateral displacement upon direct physical contact with a micropillar. Multiple instances of the cell–pillar contact can accumulate as a significant lateral shift of the cell. In the device design stage, we first adopted THP-1 cells in culture media as our test samples, and a successful cell focusing operation in medium is described in Fig. 2a and ESI† Video S1. To optimize the device for high-yield cell isolation, we have examined arrangements of the focusing micropillars and the

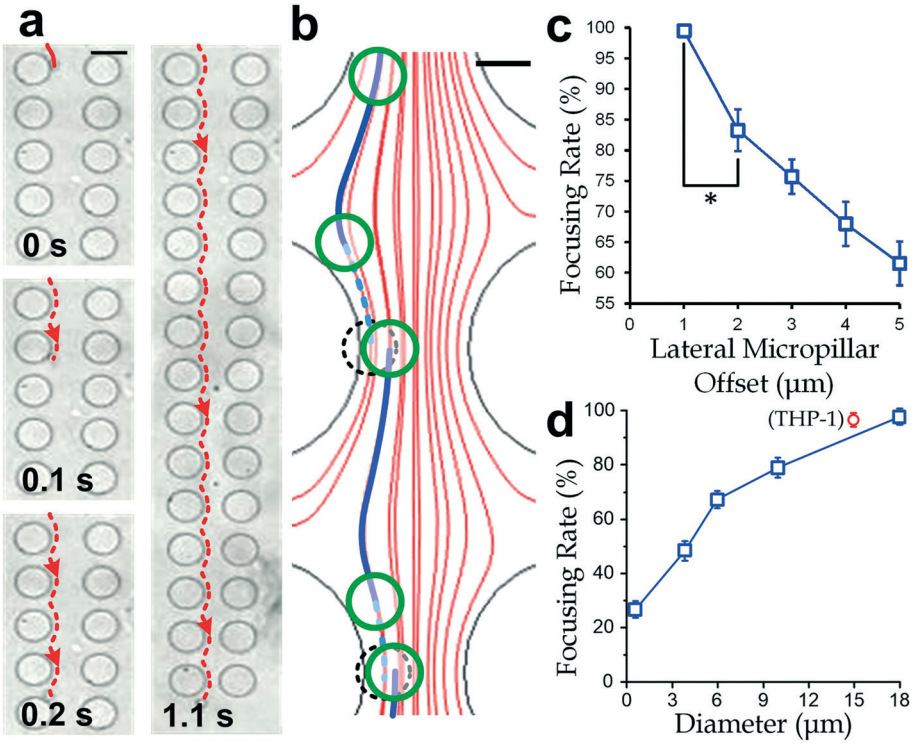

Fig. 2 (a) Trajectory of a cell flowing in a focusing module. The snapshots at 0 s, 0.1 s and 0.2 s show the region between the 23rd to 27th micropillars; and the snapshot at 1.1 s shows the region between the 23rd to 35th micropillars. Scale bar: 50 μm. (b) Simulated velocity profile and streamlines (red). When a cell is in contact with the micropillars, the cell has to be shifted aside, indicated by the lateral distance between the dotted circles and the nearest green circles. Scale bar: 10 μm. (c) Focusing rate for devices with different lateral micropillar offsets (N = 10 for each point). (d) Focusing rate for cells and microbeads with different diameters. A data point for THP-1 cells (circle) is also included (N = 10 for each point).

micro-sieves. For the cell focusing region, we considered a variety of lateral offsets of the micropillars with a fixed separating distance (70 μm) along the flow. We simulated the velocity profiles for the cell focusing modules with a lateral shifting distance of 1–5 μm, and an example (a region in the focusing region with a lateral sieve-offset of 1 μm) is provided in Fig. 2b. The simulation results have predicted that a lateral micropillar shift of 3 μm is sufficient to ensure that all the cells are being focused toward the cell focusing module exits. Further experimental analysis was implemented with the devices configured with different lateral micropillar offsets. The experiments using THP-1 cells under a forward driving pressure of 0.26 psi showed that the lateral micropillar offset should be as low as 1 μm for a high-yield (>99%) cell focusing operation (Fig. 2c). Such disagreement between the simulation and experiments on the lateral shifts could be caused by the minor effects such as cell deformation when in direct contact with the micropillars. The focusing rate for different particle sizes was also investigated. We considered the THP-1 cells and microspheres (15 μm) with different diameters (0.5 μm, 3.7 μm, 6 μm, 10.2 μm and 18 μm) as shown in Fig. 2d. Expectedly, the focusing rate increases with the particle diameter, and it can reach a reasonably high level for THP-1 cells (98.2 ± SE 0.45%). Together, the focusing micropillar array can guide cells to a specific lateral position for the subsequent cell isolation step.

In addition, it is necessary to arrange the micro-sieve positions in the cell capture region such that the cells flowing out from any position within the range of the micropillar exits were captured in the micro-sieve array. Although we had successfully adopted, in the past,[26] a micro-sieve placement scheme with alternating lateral offsets, such a scheme only worked for one column of micro-sieves with cells focused by additional side-flows. However, to achieve a higher cell isolation throughput for more general applications, an array of micro-sieves should be more preferable than a single column of the microstructures. The corresponding microfluidic conditions were apparently different, implying that the side-flows can no longer be applied; therefore, we applied the micro-pillars as the focusing units instead. Additionally, we needed to re-configure the micro-sieve arrangement as the multiple columns of micro-sieves were fluidically connected. Changing the position of one micro-sieve would vary the flow profile along the entire cell capture region. To obtain a functional micro-sieve placement configuration, we repeatedly tuned the lateral offsets from −10 to 10 μm for each micro-sieve and simulated flows in the entire capture region (a region of simulated flow profiles in the capture region is available in Fig. 3a). Briefly, we traced

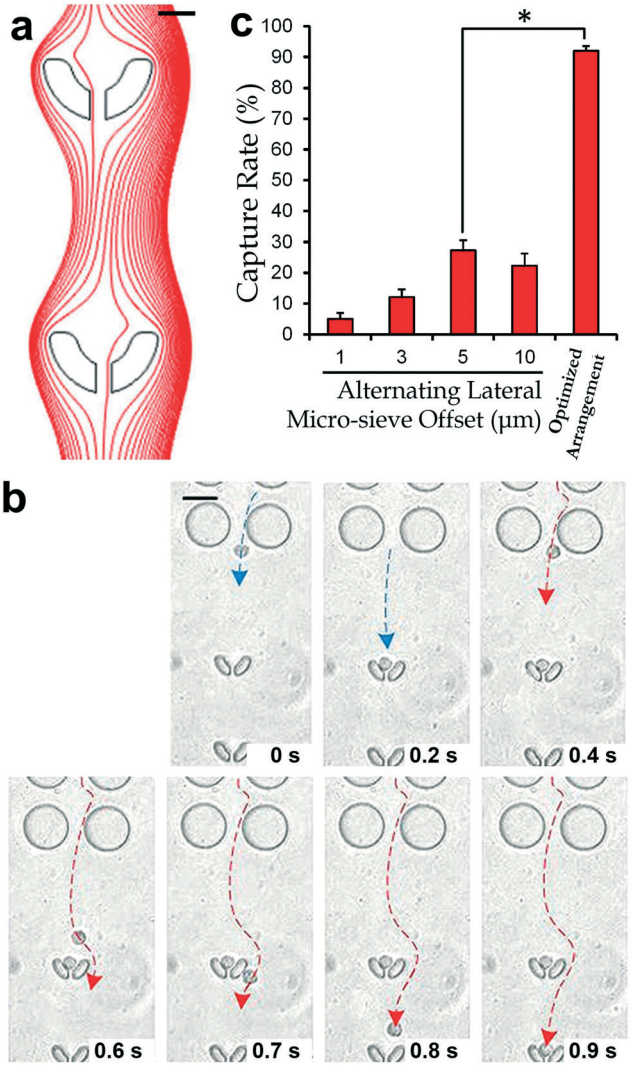

Fig. 3 (a) Simulated streamlines around two micro-sieves. Scale bar: 15 μm. (b) Trajectories of two cells flowing and being captured in the first two micro-sieves in the capture region, with blue dashed lines and red dashed lines representing the trajectories of the first cell and the second cell, respectively. Scale bar: 50 μm. (c) Capture rates of the capture region for different micro-sieve arrangements (N = 10 for each point).

the cell trajectories of all the possible positions from the focusing module exits. We would consider that a lateral cell shift was induced around the micro-sieve regions. We carefully adjusted the micro-sieve placement such that they covered the maximum range of streamlines coming out from the corresponding upstream focusing module, and we obtained a cell capture rate of >95% based on simulation. The resultant micro-sieve configuration is described in Table S1.† For further verification, we performed the cell isolation experiment with the THP-1 cells, which were pretreated with 50 ng ml^{-1} phorbol 12-myristate 13-acetate (PMA; Sigma-Aldrich) for 48 h for macrophage differentiation and induction of CD14 expression on the cells.[38,39] Thus, the PMA-treated THP-1 cells can represent the CD14 expressing immune cells, such as monocytes and macrophages in tissues. An example of the cell trajectories during the experiment is shown in Fig. 3b. This 'optimized' design achieved a significantly improved capture rate of 92 ± SE 1.3% (Fig. 3c). The reduced capture rate compared to that from the simulation was likely caused by the cell deformation and any alteration of flow profiles in the presence of cells.

Effects of driving pressure levels

We further investigated the driving pressure for the cell isolation operation. The PMA treated THP-1 cells (density: 10^6 cells per ml; volume: 1 μl) were injected into the device with different driving pressures, ranging from 0.22 psi to 0.3 psi. The trajectories of THP-1 cells flowing into the device were recorded and the cells flowing out from the focusing module were counted, whether or not the cells came out from the module exits. For instance, the cells, which were not successfully focused, escaped through the gaps between the consecutive micropillars and flowed outside the module exits. We quantified the focusing rate as the number of cells flowing out from the focusing module exits relative to the total number of injected cells. The results (Fig. 4a) show that the focusing rate was maintained to be >99% in the tested pressure range. On the other hand, the cells flowing in the capture region were also recorded (see ESI† Video S2†), and the capture rate was calculated by counting the number of cells captured by the micro-sieves relative to the total cells in the region. The cell capture rate reached the maximum level (91.5 ± SE 1.27%) at a driving pressure of 0.26 psi for a flow rate of 6.78 μl min^{-1} (measured by weighing the liquid coming out from the device outlet under a steady driving pressure of 0.26 psi over 30 min) as shown in Fig. 4b. It is possible that a lower driving pressure was insufficient to overcome the binding between the cells and the inner surfaces of the device, whereas an excessive pressure could induce cell deformation and variation of the cell trajectories.

We have also examined the attachment of the bound THP-1 cells in micro-sieves using the backward flow pressure levels. As shown in Fig. 4c, under a pressure of <1 psi, all the THP-1 cells could stay in the micro-sieves. When the pressure increases, some cells were removed from the micro-sieves; example snapshots of the cell detachment process are shown in the inset of Fig. 4c. All the attached cells were removed under a pressure of 5 psi. As a control case, we have repeated the experiments using the device coated with cell-repelling molecules (Pluronic F-127, 9003-11-6, Sigma-Aldrich, St. Louis, Missouri, USA) instead of the antibodies to eliminate the cell-specific binding. All the captured cells in micro-sieves were removed by a backward pressure of ≥0.5 psi, indicating that the cell–sieve adhesion was caused by the specific antibody binding to CD14. Thereby, in the cell isolation procedures using the device, we adopted a backward pressure of 1 psi for removing the untargeted cells, and a backward pressure of 5 psi for extracting the targeted cell type.

On the one hand, we have performed experiments to verify the viability of the isolated cells, which is >99% after

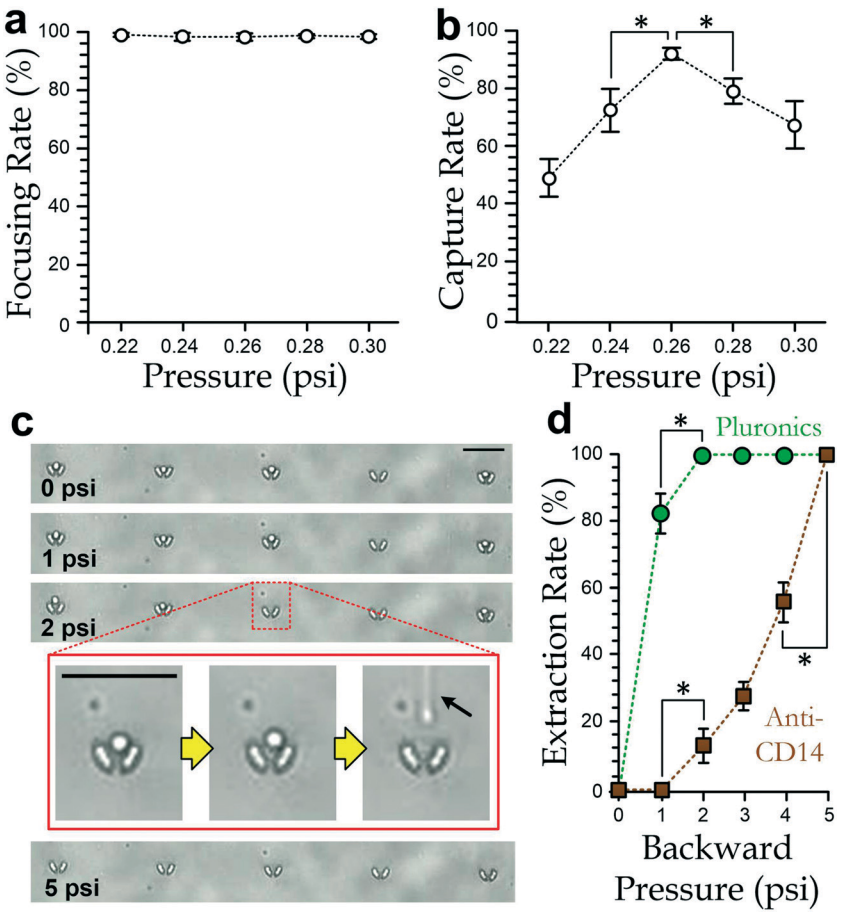

Fig. 4 (a) Focusing rate and (b) capture rate for different forward driving pressure levels. At least ten devices have been tested for each bar in both charts. (c) Presence of the captured PMA-treated THP-1 cells in the anti-CD14 coated micro-sieves under different backward pressure levels. Inset: A cell detaches and leaves a micro-sieve under the backward pressure. The moving cells were taped as a blurry line in the video (arrow). Scale bar: 100 μm. (d) Extraction rate of specifically bound THP-cells under different backward pressure levels for the anti-CD14-coated microstructures and the Pluronic-coated microstructures as the control case (N = 8 for each point, except those with 0% extraction rate).

extracting the bound cells using a backward pressure of 5 psi; hence, such cell extraction should not cause noticeable cell death. On the other hand, when the cells are continuously incubated in the device for a duration of up to 24 h, the cell viability can be maintained, >98%, reflecting the potential of this device for any further cell processes and analyses directly inside the device in any further applications.

Cell isolation from blood

The microfluidic device can support the isolation of immune cells in a liquid sample. Though immune cells typically have a density of 4×10^6–1×10^7 cells per ml in blood,[40] there are other cells present in blood including red blood cells with a hematocrit level of ~45%. It is well known that such a high density of red blood cells can interfere with the trajectories of white blood cells when flowing both cells together,[41] compared to the trajectories of white blood cells flowing alone. Though the cell isolation scheme works well for cells in culture media at a relatively low cell density, we should investigate the effect of the blood hematocrit level on the presented scheme. We have conducted experiments on bovine blood samples containing immune cells with a known density. We first filtered out the bovine immune cells from the bovine blood using a nylon syringe filter as described in Materials and methods. We adjusted the hematocrit level by simple dilution with PBS. Next, we added THP-1 cells with a density of 10^6 cells per ml into the diluted blood, reaching a hematocrit level ranging from 5% to 40%. Each biosample was injected into the cell isolation device under a pressure of 0.26 psi and the cell trajectories along the microstructures were captured. As an example, snapshots of an immune cell trajectory in the diluted blood are shown in Fig. 5a. Expectedly, the results show that both the focusing rate (Fig. 5b) and capture rate (Fig. 5c) decrease with the hematocrit level because a lower hematocrit level implies a larger separating distance and the weaker disturbance of red blood cells to the THP-1 cell trajectory. In particular, a hematocrit level of ≤10% would result in a focusing rate of >93.2% and a capture rate of >77.5%. For practical implementation, we suggest that the blood samples should be diluted to a hematocrit level of ≤10% with PBS for the

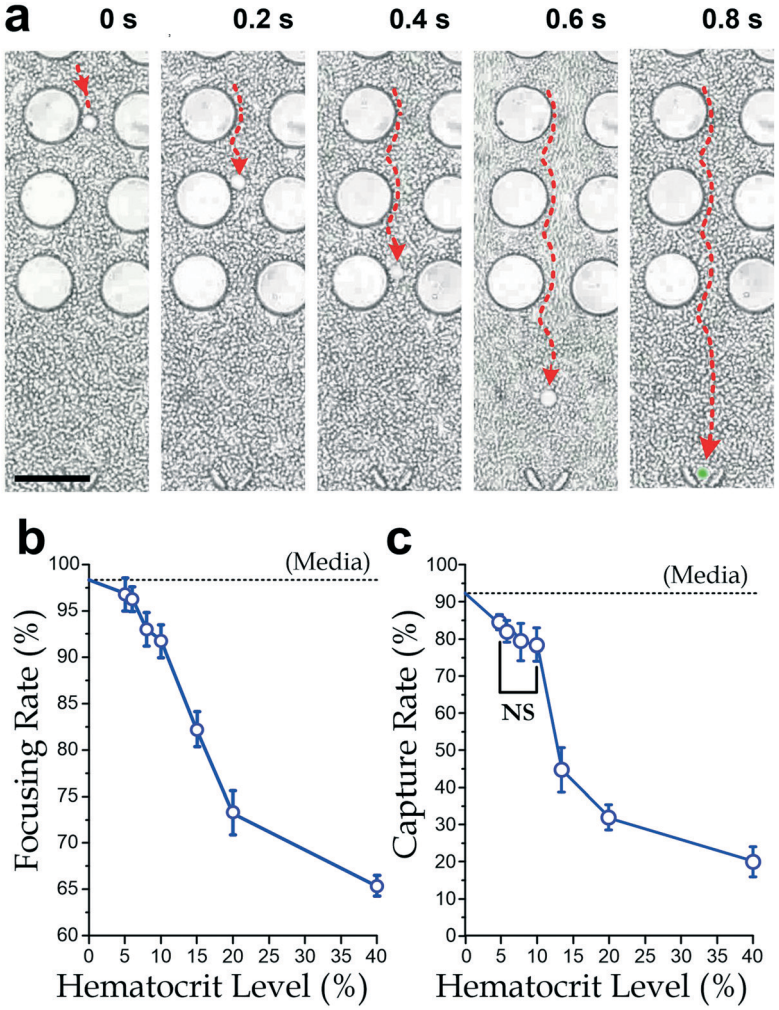

Fig. 5 (a) Trajectory of a THP-1 cell flowing in diluted blood (dilution ratio: 1 : 3) along the microstructures at 0 s, 0.2 s, 0.4 s, 0.6 s, and 0.8 s. A fluorescence micrograph of the isolated THP-1 cell (green) is combined with the snapshot at 0.8 s. Scale bar: 70 μm. (b) Focusing rate and (c) isolation rate of THP-1 cells for different blood dilution ratios ($N \geq 10$ for each point). The rates for THP-1 cells in pure culture media (0% hematocrit level) are indicated by the dashed lines.

reported cell isolation scheme. It should also be noted that the adopted immune cell density of 10^6 cells per ml at a hematocrit level of 10% is equivalent to an immune cell density of $\sim 4.5 \times 10^6$ in the whole blood, falling within the normal range as in human blood.

Target cell type extraction

We implemented multiple operation runs with the micro-structured device to isolate a CD14-expressing immune cell type from a cell mixture. To prepare the biosample, we mixed PMA-treated THP-1 cells (average diameter: 15 μm; density: 2×10^5 cells per ml), MDA-MB-231 cells (average diameter: 17 μm; density: 8×10^5 cells per ml) and diluted blood (hematocrit level: ~10%). As a demonstration of the device procedures, we chose MDA cells to represent the untargeted cells as they do not express the CD14 surface protein, and they are expected to have an equivalent cell isolation result as other CD14-negative immune cells. To better distinguish the cell types, we stained only the THP-1 cells with fluorescent dye (Cell Tracer kit, V12883, Thermo Fisher Scientific, Waltham, Massachusetts, USA). During the biosample injection (total density: 10^4 cells per ml; volume: 1 μl) under a steady inlet pressure of 0.26 psi, we monitored the downstream position of the capture region to count any cells bypassing the micro-sieve array, followed by checking the cells captured in the micro-sieves after a PBS flush from the inlet (Fig. 6a, left). The red blood cells could easily deform[42] and escape the micro-sieve structure during the PBS flush. Considering that the filtered blood contained no cells with a diameter of >7 μm, the isolated cells in the micro-sieves are either THP-1 (with fluorescence) or MDA (without fluorescence). Since these two cell types have a comparable size, most of them were captured in the micro-sieve array, with ~19.1% of the cells escaping the microstructures without being captured (Fig. 6b). After a brief incubation of 10 min to facilitate the CD14–antibody binding, we applied a backward pressure of 1 psi to remove and collect the

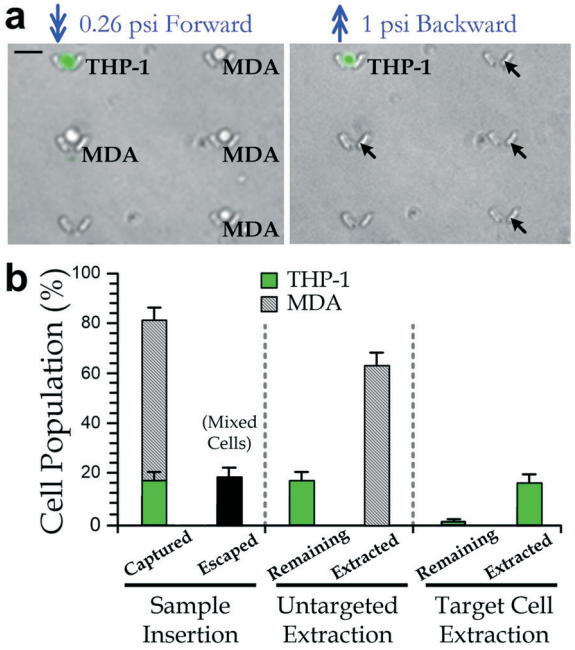

Fig. 6 (a) A micro-sieve region during the sample insertion step (left) and the untargeted cell extraction step (right). A biosample containing both the MDA cells and the pre-stained PMA-treated THP-1 cells (green) in bovine blood with ~10% hematocrit level is used. The arrows indicate the cell removal under a backward pressure of 1 psi. Scale bar: 50 μm. (b) Statistics of cell counts relative to the total inserted cell population in the different steps of the specific cell isolation operation. At least 10 repeated cell isolation experiments were performed to quantify the THP-1 cells and MDA cells.

unbound cells (see ESI† Video S3). The fluorescence-stained THP-1 cells (~16.4% of the injected cells) could remain in the micro-sieves (Fig. 6a, right), whereas all the untargeted MDA cells (~64% of the total injected cells as shown in Fig. 6b) were removed by the backward flow. Next, we increased the backward pressure to 5 psi (inducing a backward flow rate of 35.4 μl min^{-1}) for 2 min to extract the target THP-1 cells with specific protein–antibody binding, and then we counted any cells in the micro-sieves. We have observed some captured THP-1 cells (~0.32% of the injected cells) that remained in the micro-sieves. In summary, most of the target cells can be extracted successfully (98% of the captured THP-1 cells), which could be further reduced by increasing the duration and level of the backward pressure. Furthermore, we have performed viability tests on the extracted THP-1 cells, obtaining a viability of 93%. Such a reduced viability (compared to 98% for the cells in the device) can be possibly explained by physical damage to the cell membranes, caused by the higher backward pressure (5 psi) applied to break the antibody–antigen bonds between the target cells and micro-sieves. This experiment demonstrates the isolation of a target immune cell subtype from a cell mixture. From all our experiment runs, we have not observed any MDA cells staying in the micro-sieve and any removal of bound THP-1 cells during the untargeted cell extraction step, indicating the high yield and high purity of the isolated cell types. With the current microstructure arrangement, the overall isolation rate of the target cells in the diluted blood is ~80% (*i.e.* the 80.1% capture rate multiplied by the 98% extraction rate). Notably, such an isolation rate can be further enhanced by collecting the 'escaped' cells at the device outlet and applying the cell isolation procedures again with these cells, yet a long time of processing would be a trade-off.

In future device development, the current capture region (~2 mm wide and ~2 mm long) can be further extended to include more focusing modules and more micro-sieves for processing a larger volume of biosamples. For example, we can fabricate a much larger area of the microstructures on a 50 mm × 75 mm glass slide with 200 focusing modules (~40 mm wide) and 200 × 600 micro-sieves (~60 mm long) for isolating ~10^5 cells from a biosample. Expectedly, a wider flow channel of 40 mm can then support a higher throughput of ~44 μl min^{-1} for raw blood samples for more general immune cell isolation applications.

Considering the target application of the reported cell isolation strategy on raw human blood, white blood cells (WBCs) such as macrophages, neutrophils, lymphocytes, and basophils can be captured and bound to the antibody-coated surfaces of the micro-sieves. The surface protein expressions are sometimes non-specific, *i.e.* multiple immune cell subtypes express the same surface protein.[43,44] For example, both neutrophils and macrophages express CD14, causing neutrophils to be present with the resultant cells from the isolation of THP-1.[45] Though the surface protein expressions do not guarantee the absolute specificity of identifying an immune cell subtype, the extracted target cells can be subsequently isolated using multiple devices with other antibody coatings for a more specific cell subtype. For example, macrophages can be isolated with an anti-CD14 coated device and then an anti-CD16a coated device.[46] The extracted untargeted cells from the CD14-based isolation can be collected and passed to another device with the anti-CD16a coating for a secondary cell isolation run. The cell isolation specificity can be enhanced to a certain extent in this way.

We have performed further tests with the unfiltered bovine blood with a dilution ratio of 1 : 3 in PBS. We have confirmed that a backward flow of 1 psi can remove all the blood cells captured in the micro-sieves from a cell isolation device without an antibody coating, indicating that the non-specific bindings between the cells and micro-sieves can be neglected.

Furthermore, though it is well known that different cell subtypes can have a common surface protein expression, but their expression levels can be different. For instance, T-cells, dendritic cells, and platelets are CD14-negative, but neutrophils and B lymphocytes may have a low detectable level of CD14 expression.[47] Monocytes and most macrophages exhibit stronger CD14 expression. This implies that different immune cell subtypes can also be distinguished with different cell extraction rates using the cell isolation devices, yet the extraction of different cell subtypes requires further development and optimization of

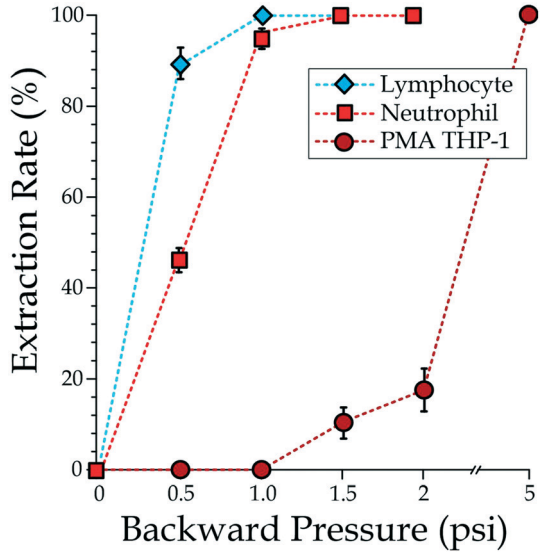

Fig. 7 Extraction rates of PMA-treated THP-1 cells, lymphocytes and neutrophils (from bovine blood) captured in the micro-sieves under different backward pressure levels ($N \geq 4$ for each error bar).

the protocols of the cell isolation device. To achieve even higher cell isolation specificity, we propose to apply 1) multiple cell isolation devices with different antibody coatings as previously discussed and 2) different levels of backward pressure for each device to extract cells with similar expression ranges of a particular surface protein. In order to demonstrate the feasibility of cell subtype extraction, here, we have performed a set of experiments to characterize the extraction rates of immune cells as a function of the backward pressure. In these experiments, we prepared the sample using unfiltered diluted bovine blood mixed with PMA-treated THP-1 cells (2×10^5 cells per ml), which were pre-stained with fluorescent GFP as previously described. We performed the cell capture procedures with an anti-CD14-coated cell isolation device, and identified the captured THP-1 cells in the micro-sieves. Next, we stained all the other captured cells using a Wright–Giemsa Stain kit (9990716, Thermo Fisher Scientific, Waltham, Massachusetts, USA). We then examined the staining conditions of these captured cells to determine bovine leukocytes and neutrophils, followed by applying a backward flow from a pressure of 0.5 psi to 2 psi. The leukocytes appeared in blue-purple whereas the neutrophils contained lavender granules in the cytoplasm. By identifying each micro-sieve with a cell extracted at different pressure levels, we obtained their accumulative extraction rates for different pressure levels as shown in Fig. 7. Under a backward pressure of 1 psi, all the captured lymphocytes and ~93% of the captured neutrophils can be extracted, agreeing with previous studies.[48] All the THP-1 cells were removed with a backward pressure of up to 5 psi. This implies that we can establish a protocol with a lower backward pressure (~1–2 psi) to remove the cells exhibiting weaker CD14-expression, followed by applying a higher backward pressure level (~5 psi) to extract the cells exhibiting stronger CD14-expression, such as macrophages and PMA-treated THP-1 cells. Future development of the reported immune cell isolation strategy should include the detailed protocols based on the devices with different antibody coatings and regulation of the backward pressure levels.

Conclusion

In this paper, we report a micro-structured device for high-yield specific isolation of immune cells from multiple-cell-type biosamples in either culture media or diluted blood. We applied rows of micropillars for cell focusing and a micro-sieve array for the subsequent cell isolation. The arrangements of these microstructures have been optimized by both simulation analysis and experiments, achieving a focusing rate of >95% and cell capture yield of ~85% for immune cells in culture media. Isolation of a target immune cell subtype can be achieved by the specific cell surface protein binding on the antibody-coated microstructure surfaces. This work has further demonstrated that the target PMA-treated THP-1 cells can be isolated from a multiple cell-type mixture in diluted blood with a yield rate of >80% while the cell viability (>93%) can be maintained. Such a reduction of the isolation yield for the blood sample is possibly caused by the presence of a high density of red blood cells. The detailed cell isolation procedures can be further configured to enable the extraction of multiple defined immune cell subtypes using devices with different antibody coatings and multiple backward pressure levels. The focusing micro-pillars and micro-sieve array can also be expanded as a larger flow region with the repeated microstructures for processing a high-throughput of cell isolation, meeting the requirements of specific immune cell isolation from clinical samples for a wide range of healthcare/medical applications.

Author contributions

J. Li performed most of the experiments. Y. Liu designed the device and conducted simulations and the preliminary experiments. J. Ren fabricated the device. B. Z. Tay performed simulations. T. Luo maintained the cells. L. Fan prepared the experiments, including the blood. D. Sun provided advice. G. Luo helped in the literature review. D. Lau provided advice and arranged the experiments for the isolation of bovine immune cells. Marcos provided advice, especially on the device design optimization. R. H. W. Lam came up with the research idea and provided advice.

Conflicts of interest

There are no conflicts to declare.

Acknowledgements

We acknowledge the financial support from the National Natural Science Foundation of China (NSFC 31500758), and the Hong Kong Research Grant Council (GRF 11204317).

References

1 P. J. Delves and I. M. Roitt, *N. Engl. J. Med.*, 2000, **343**, 37–49.
2 J. Ermann and C. G. Fathman, *Nat. Immunol.*, 2001, **2**, 759.
3 F. Abali, M. Stevens, A. G. J. Tibbe, L. Terstappen, P. N. van der Velde and R. B. M. Schasfoort, *Anal. Biochem.*, 2017, **531**, 45–47.
4 B. Moser and P. Loetscher, *Nat. Immunol.*, 2001, **2**, 123.
5 C. W. Shields IV, C. D. Reyes and G. P. López, *Lab Chip*, 2015, **15**, 1230–1249.
6 A. A. Adams, P. I. Okagbare, J. Feng, M. L. Hupert, D. Patterson, J. Göttert, R. L. McCarley, D. Nikitopoulos, M. C. Murphy and S. A. Soper, *J. Am. Chem. Soc.*, 2008, **130**, 8633–8641.
7 E. D. Pratt, C. Huang, B. G. Hawkins, J. P. Gleghorn and B. J. Kirby, *Chem. Eng. Sci.*, 2011, **66**, 1508–1522.
8 A. J. Link, K. J. Jeong and G. Georgiou, *Nat. Rev. Microbiol.*, 2007, **5**, 680–688.
9 Y. Cui, Q. Wei, H. Park and C. M. Lieber, *Science*, 2001, **293**, 1289–1292.
10 J. Gille, S. Wallstabe, A. P. Schulz, A. Paech and U. Gerlach, *J. Orthop. Surg. Res.*, 2012, **7**, 20.
11 G. Perozziello, R. La Rocca, G. Cojoc, C. Liberale, N. Malara, G. Simone, P. Candeloro, A. Anichini, L. Tirinato, F. Gentile, M. L. Coluccio, E. Carbone and E. Di Fabrizio, *Small*, 2012, **8**, 2886–2894.
12 R. He, L. Zhao, Y. Liu, N. Zhang, B. Cheng, Z. He, B. Cai, S. Li, W. Liu, S. Guo, Y. Chen, B. Xiong and X. Z. Zhao, *Biomed. Microdevices*, 2013, **15**, 617–626.
13 J. A. Phillips, Y. Xu, Z. Xia, Z. H. Fan and W. Tan, *Anal. Chem.*, 2009, **81**, 1033–1039.
14 S. Sharma, J. Zapatero-Rodriguez, P. Estrela and R. O'Kennedy, *Biosensors*, 2015, **5**, 577–601.
15 E. K. Sackmann, A. L. Fulton and D. J. Beebe, *Nature*, 2014, **507**, 181–189.
16 W. R. Rodriguez, N. Christodoulides, P. N. Floriano, S. Graham, S. Mohanty, M. Dixon, M. Hsiang, T. Peter, S. Zavahir, I. Thior, D. Romanovicz, B. Bernard, A. P. Goodey, B. D. Walker and J. T. McDevitt, *PLoS Med.*, 2005, **2**, e182.
17 W. Chen, N. T. Huang, B. Oh, R. H. W. Lam, R. Fan, T. T. Cornell, T. P. Shanley, K. Kurabayashi and J. Fu, *Adv. Healthcare Mater.*, 2013, **2**, 965–975.
18 T. Endo, K. Kerman, N. Nagatani, H. M. Hiepa, D.-K. Kim, Y. Yonezawa, K. Nakano and E. Tamiya, *Anal. Chem.*, 2006, **78**, 6465–6475.
19 S. Nagrath, L. V. Sequist, S. Maheswaran, D. W. Bell, D. Irimia, L. Ulkus, M. R. Smith, E. L. Kwak, S. Digumarthy and A. Muzikansky, *Nature*, 2007, **450**, 1235.
20 T. Huang, C. P. Jia, Y. Jun, W. J. Sun, W. T. Wang, H. L. Zhang, H. Cong, F. X. Jing, H. J. Mao, Q. H. Jin, Z. Zhang, Y. J. Chen, G. Li, G. X. Mao and J. L. Zhao, *Biosens. Bioelectron.*, 2014, **51**, 213–218.
21 K. Loutherback, J. Puchalla, R. H. Austin and J. C. Sturm, *Phys. Rev. Lett.*, 2009, **102**, 1–4.
22 T. J. Bowman, G. Drazer and J. Frechette, *Biomicrofluidics*, 2013, **7**, 64111.
23 K. Loutherback, K. S. Chou, J. Newman, J. Puchalla, R. H. Austin and J. C. Sturm, *Microfluid. Nanofluid.*, 2010, **9**, 1143–1149.
24 M. E. Warkiani, B. L. Khoo, L. Wu, A. K. P. Tay, A. A. S. Bhagat, J. Han and C. T. Lim, *Nat. Protoc.*, 2016, **11**, 134–148.
25 S. Wang, A. Thomas, E. Lee, S. Yang, X. Cheng and Y. Liu, *Analyst*, 2016, **141**, 2228–2237.
26 Q. D. Tran, T. F. Kong, D. Hu and R. H. Lam, *Lab Chip*, 2016, **16**, 2813–2819.
27 M. Khan and S.-Y. Park, *Colloids Surf., B*, 2015, **127**, 241–246.
28 C. Chen, J. Skog, C.-H. Hsu, R. T. Lessard, L. Balaj, T. Wurdinger, B. S. Carter, X. O. Breakefield, M. Toner and D. Irimia, *Lab Chip*, 2010, **10**, 505–511.
29 J. P. Gleghorn, E. D. Pratt, D. Denning, H. Liu, N. H. Bander, S. T. Tagawa, D. M. Nanus, P. A. Giannakakou and B. J. Kirby, *Lab Chip*, 2010, **10**, 27–29.
30 Z. Du, N. Colls, K. Cheng, M. Vaughn and L. Gollahon, *Biosens. Bioelectron.*, 2006, **21**, 1991–1995.
31 B. Song, V. Sivagnanam, C. D. Vandevyver, I. Hemmilä, H.-A. Lehr, M. A. Gijs and J.-C. G. Bünzli, *Analyst*, 2009, **134**, 1991–1993.
32 S. M. Opal, J. E. Palardy, N. Parejo and R. L. Jasman, *Crit. Care Med.*, 2003, **31**, 929–932.
33 L. M. Weber, K. N. Hayda, K. Haskins and K. S. Anseth, *Biomaterials*, 2007, **28**, 3004–3011.
34 Y. Jin, T. Zhang, Y. Samaranayake, H. Fang, H. Yip and L. Samaranayake, *Mycopathologia*, 2005, **159**, 353–360.
35 M. Berney, F. Hammes, F. Bosshard, H.-U. Weilenmann and T. Egli, *Appl. Environ. Microbiol.*, 2007, **73**, 3283–3290.
36 H. Li and R. Bashir, *Sens. Actuators, B*, 2002, **86**, 215–221.
37 I. Barbulovic-Nad, H. Yang, P. S. Park and A. R. Wheeler, *Lab Chip*, 2008, **8**, 519–526.
38 T. Kohro, T. Tanaka, T. Murakami, Y. Wada, H. Aburatani, T. Hamakubo and T. Kodama, *J. Atheroscler. Thromb.*, 2004, **11**, 88–97.
39 S. Tedesco, F. De Majo, J. Kim, A. Trenti, L. Trevisi, G. P. Fadini, C. Bolego, P. W. Zandstra, A. Cignarella and L. Vitiello, *Front. Pharmacol.*, 2018, **9**, 71.
40 G. J. Tortora and B. Derrickson, *Principles of anatomy & physiology*, Wiley, Hoboken, NJ, 13th edn, 2012.
41 F. Pierige, S. Serafini, L. Rossi and A. Magnani, *Adv. Drug Delivery Rev.*, 2008, **60**, 286–295.
42 M. R. Hardeman, G. A. J. Besselink, I. Ebbing, D. de Korte, C. Ince and A. J. Verhoeven, *Transfusion*, 2003, **43**, 1533–1537.
43 P. R. Wheater, *Functional histology : a text and colour atlas*, ed. P. R. Wheater and H. G. Burkitt, Edinburgh: Churchill Livingstone, Edinburgh, 2nd edn, 1987.
44 H. Harjunpaa, M. L. Asens, C. Guenther and S. C. Fagerholm, *Front. Immunol.*, 2019, **10**, 1078.
45 A. Haziot, B. Z. Tsuberi and S. M. Goyert, *J. Immunol.*, 1993, **150**, 5556–5565.
46 N. Inohara and G. Nuñez, *Nat. Rev. Immunol.*, 2003, **3**, 371.
47 P. Antal-Szalmas, J. A. Strijp, A. J. Weersink, J. Verhoef and K. P. Van Kessel, *J. Leukocyte Biol.*, 1997, **61**, 721–728.
48 J. Hussen and H.-J. Schuberth, *Front. Immunol.*, 2017, **8**, 1875.